Structural Engineering and Mechanics, *Vol. 74, No. 4 (2020) 521-532*
DOI: https://doi.org/10.12989/sem.2020.74.4.521

Ballasting plan optimization for operation of a 2D floating dry dock

Kyungho Yoon[1], Hyo-Jin Kim[1], Seungkyun Yeo[1], Younghwa Hong[2], Jihye Cha[2] and Hyun Chung *[3]

[1]Department of Mechanical Engineering, Korea Advanced Institute of Science and Technology, 291, Daehak-ro, Yuseong-gu, Daejeon 34141, Republic of Korea
[2]Institute of Industrial Technology, Samsung Heavy Industries, 217, Munji-ro, Yuseong-gu, Daejeon 34051, Republic of Korea
[3]Department of Naval Architecture & Ocean Engineering, Chungnam National University, 99, Daehak-ro, Yuseong-gu, Daejeon 34134, Republic of Korea

(Received December 18, 2019, Revised December 19, 2019, Accepted December 26, 2019)

Abstract. A floating dry dock is an advanced structure that can provide a solution for dry dock space shortages. The critical point in floating dock operation is compensating the deflection caused by a heavy payload by adjusting the water level in the ballast system. An appropriate ballasting plan warrants safe and precise construction on a floating dock. Particularly, in the case of a 2D floating dock, ballasting plan evaluation is crucial due to complex deformation modes. In this paper, we developed a method to calculate the optimal ballasting plan for accurate and precise construction on a 2D floating dock. The finite element method was used for considering the flexibility of the floating dock as well as the construction blocks. Through a gradient-based optimization algorithm, the optimal ballasting plan for the given load condition was calculated in semi-real time (5 min). The present method was successfully used for the actual construction of an offshore structure on the 2D floating dock.

Keywords: floating dock; offshore structure; finite element model; optimization; ballasting plan

1. Introduction

A floating (dry) dock is a barge-shaped floating structure with a ballast system for shipbuilding and construction of offshore structures in the maritime environment. Because dock space capacity is a primary factor in determining the entire construction schedule, securing space can increase productivity. A floating dock does not require yard space on the ground and is therefore being widely used as a solution for dock space shortages in various fields of ocean engineering (Shan *et al*. 2009, Germanischer Lloyd 1993, American Bureau of Shipping 2009, China Classification Society 2009, Det Norske Veritas 2012, Russian Maritime Register of Shipping 2014).

During the construction process on a floating dock, safety and precision controls should be managed more carefully since the work space is subject to deflections and inclination due to the heavy and uneven load conditions as well as the floating conditions at sea. To compensate for deformation and to maintain work space flatness, the floating dock typically has a ballast system composed of multiple ballast tanks. The amount of water in each ballast tank is adjusted to control the weight distribution of the floating dock. For the effective operation of the ballast system, it is crucial to provide accurate and reliable information to operators about the current dock state. Research has been conducted to develop a system for monitoring the deflection and inclination of floating docks (Yang *et al*. 2013, Korotaev *et al*. 2016, Smith and LeVezu 2012). Although these systems have been successfully used in on-site floating dock operation, there remains a critical limitation in that the final decision for a ballasting plan should depend on the intuition of experienced operators. A method was proposed for providing an optimal ballasting plan without an intuitive decision from an operator (Kurniawan and Ma 2009), but this method is still limited to load-out operations for 1D floating docks, on which ballast tanks are arranged only in the longitudinal direction.

Recently, the construction of offshore structures such as semi-submersible tension leg platforms has posed a challenge to the use of 2D floating docks. Unlike conventional 1D floating docks for shipbuilding, a 2D floating dock has complicated deformation modes as well as a matrix array ballast system. Due to this complexity, it is difficult to depend on intuitive decisions even when information about deflection and inclination is known. For accurate control of construction on a 2D floating dock, an appropriate ballasting plan should be provided to the operators.

In this paper, we propose a method for determining the optimal ballasting plan for safe and precise operation of a 2D floating dock. The flexibilities of the dock and the construction blocks (i.e., the parts of the offshore structure erected on the floating dock) under hydrostatic conditions are modeled using the finite element method. The optimal ballasting plans to compensate for deflections and inclination are obtained through a gradient-based search algorithm. The proposed method was utilized as guidance software for calculating an optimal ballasting plan in semi-real time during the on-site operation of a 2D floating dock. The efficacy of the proposed method is demonstrated

∗Corresponding author, Associate Professor
E-mail: hchung@cnu.ac.kr

http://www.techno-press.com/journals/sem&subpage=7
ISSN: 1225-4568 (Print), 1598-6217 (Online)

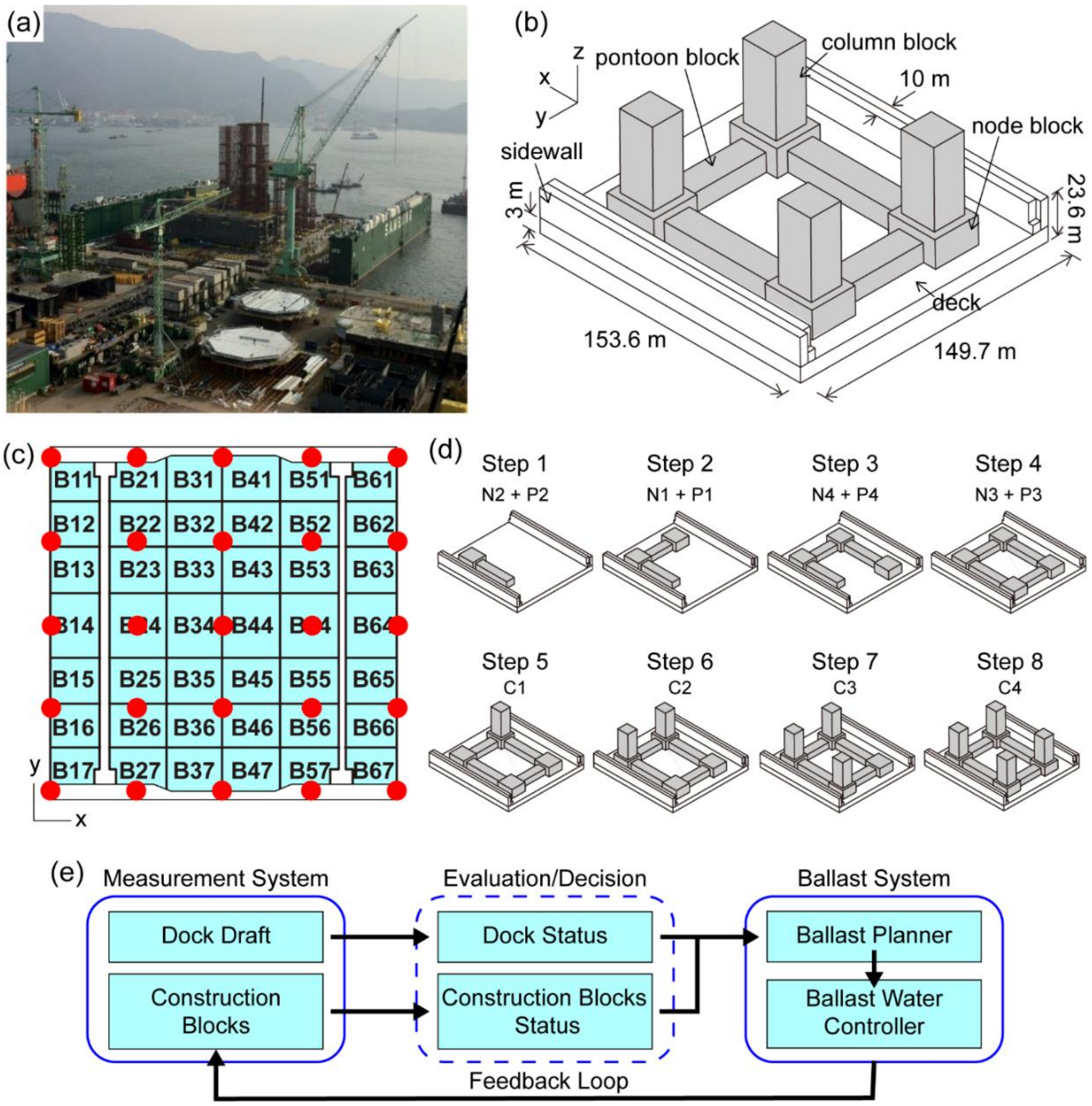

Fig. 1 Overview of 2D floating dock system. (a) Actual construction on the floating dock at pier. (b) Description of floating dock (white) and offshore structure (gray). (c) Ballast tanks layout and draft sensors locations (marked by red dots). (d) Construction steps. (e) Logic diagram of accuracy control system.

through actual application in the construction of the Jack & Saint Malo (JSM) offshore platform.

This paper is organized as follows. In Section 2, we give a brief introduction to the specifications of the 2D floating dock that was used and the construction process. In Section 3, we present the simplified finite element model and the optimization method. In Section 4, we show the calibration results of the finite element model and in Section 5 we show the numerical results of calculating the optimal ballasting plan for the construction process. Section 6 presents the on-site application of the proposed method and finally, we conclude with a summary in Section 7.

2. System overview

The construction of the JSM was conducted while the 2D floating dock was moored at pier, where the effects of ocean waves and current are negligible, as shown in Fig. 1(a). The appropriate erection of a column block is the most critical part of the construction process because columns are prone to misalignment from even minor deck deflection. In this study, we evaluate the construction process through the erection of four column blocks.

The schematic diagram of the floating dock and the twelve construction blocks (i.e., parts of JSM), which are composed of 4 node-type blocks (N1–N4), 4 pontoon-type blocks (P1–P4), and 4 column-type blocks (C1–C4), is shown in Fig. 1(b). The floating dock consists of a rectangular deck suitable for construction of offshore structures (close to square; 149.7 × 153.6 m^2) and two side walls 23.6 m high placed at the both ends of the deck to simplify the deformation mode of the floating dock by constraining the one-directional bending behavior. The self-weight of the deck and sidewall were 26,500 and 2,000 t, respectively. Under the deck of the floating dock, forty-two

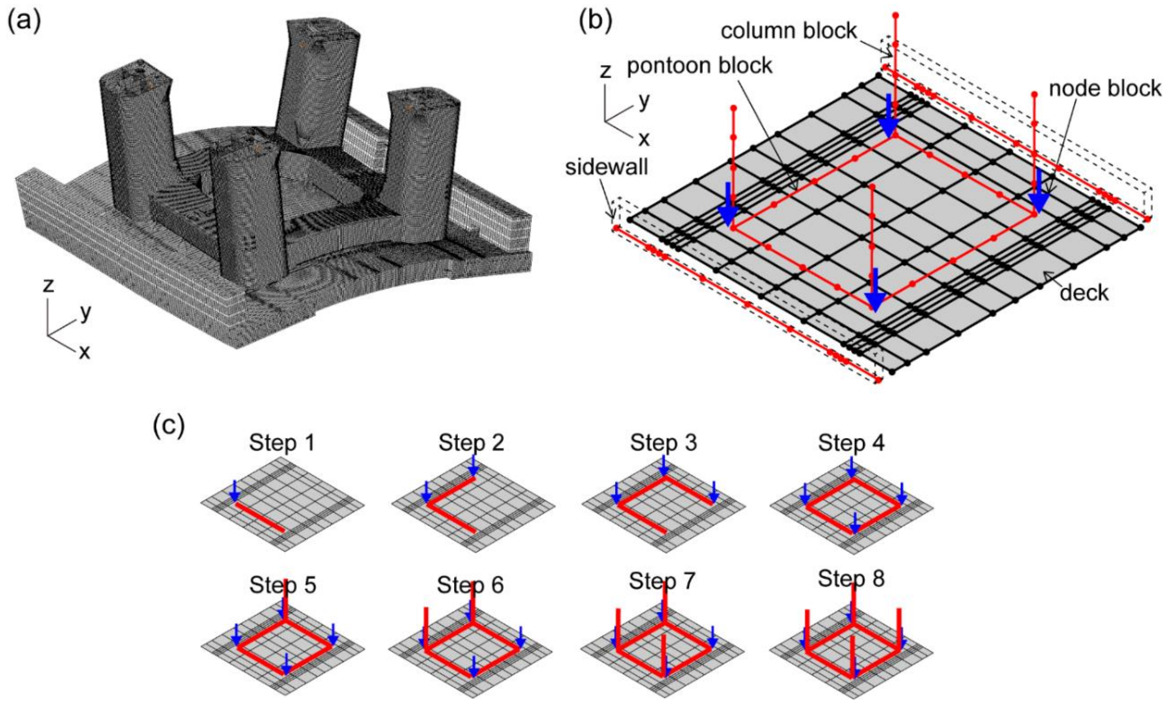

Fig. 2 Finite element model to predict deformation of the floating dock and construction blocks. (a) 3D whole structure finite element model. (b) Simplified finite element model. Gray colored rectangles indicate plate finite elements discretizing the deck of the floating dock. The red lines represent beam finite elements modeling the sidewalls, pontoon blocks, and column blocks. The blue arrows represent the force vectors induced by weight of the node blocks. (c) The simplified finite element model of each construction step.

ballast tanks are arranged as a 6 × 7 matrix (B_{11}–B_{67}, see Fig. 1(c)) to compensate for the deflection and inclination induced during the construction process. The maximum water capacity of each ballasting tank is 5,000 t. The JSM was assembled on the floating dock through 8 steps of construction process, as shown in Fig. 1(d). The dimensions and self-weight of the construction blocks for each step of the construction process are given in Table 1.

The operation system of the floating dock is divided into two parts: measurement system and ballast system (Fig. 1(e)). In the measurement system, the draft of the floating dock is measured by 25 draft sensors installed at the locations indicated by red dots in Fig. 1(c). The configurations of the construction blocks during the construction process are also monitored by an optical instrument. The ballast system consists of the ballast planner and the ballast water controller. The ballast planner generates the optimized ballasting plan for a specific purpose (i.e., stability control, local deflection, and column tip eccentricity) under the given payload condition in semi-real time (within 5 min). Then, using the ballast water controller, the amount of water in the 42 ballast tanks was adjusted according to the obtained ballasting plan.

Table 1 Specification of the construction blocks

Erection Step	ID	Dimension Width (m)	Length (m)	Height (m)	Weight (t)
1	N2	38.0	30.3	15.8	2,511.0
	P2	50.0	26.6	12.0	3,036.0
2	N1	38.0	30.3	15.8	2,511.0
	P1	50.0	28.3	12.0	3,140.0
3	N4	38.0	30.3	15.8	2,511.0
	P4	50.0	26.6	12.0	2,979.0
4	N3	38.0	30.3	15.8	2,578.0
	P3	50.0	26.0	12.0	3,097.0
5	C1	26.6	26.6	31.0	2,791.0
6	C2	26.6	26.6	31.0	2,804.0
7	C3	26.6	26.6	31.0	2,910.0
8	C4	26.6	26.6	31.0	2,921.0

3. Ballasting plan optimization

In this section, the description on the method for evaluating the optimal ballasting plan is given. The simplified finite element model is used for predicting the deflection of the floating dock. To find the optimized water amount of the ballast tanks, gradient-based optimization is used.

3.1 Finite element model

3D solid element model for the whole structure requires high computational cost with approximately tens of hours needed for a single simulation and several days needed for

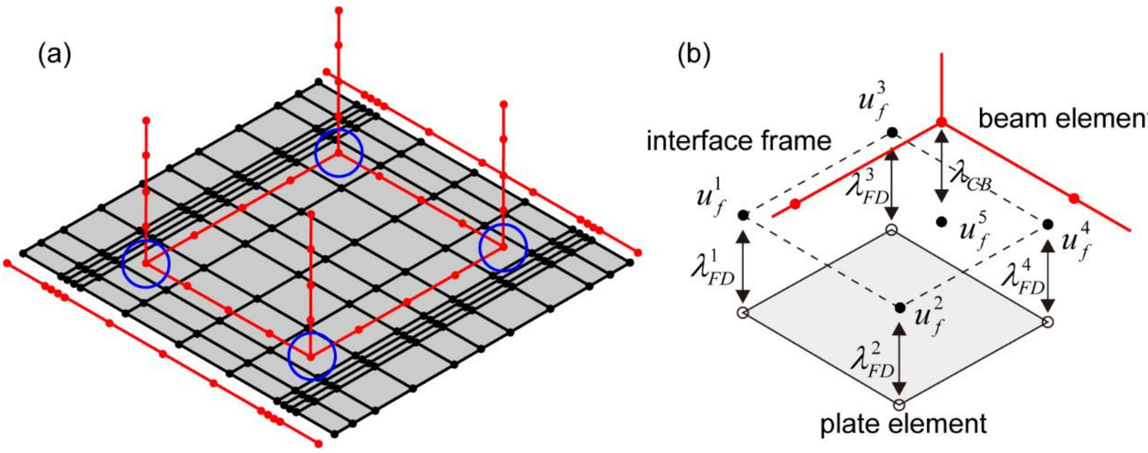

Fig. 3 Interface frames for interconnecting the floating dock (plate) and construction blocks (beam) under not-matching node conditions. (a) The blue circles show the interface frame locations. (b) The dotted rectangle and black dots indicate the interface frame and its deflection DOFs, respectively. The double-headed arrows represent Lagrange multipliers between the interface frame and the beam/plate elements.

ballasting plan optimization. To calculate the optimal ballasting plan within 5 min, we propose the simplified finite element model.

For the floating dock structures, the deck was modeled using 120 (12 × 10) MITC4 plate elements (Lee and Bathe 2002, Lee and Bathe 2004, Lee and Bathe 2005, Lee and Bathe 2010, Lee *et al*. 2012, Lee *et al*. 2014, Ko *et al*. 2016, Ko *et al*. 2017, Jun *et al*. 2018, Lee and Lee 2019) and both sides of the sidewall are modeled using 12 continuum mechanics based beam elements (Kim *et al*. 2019, Yoon *et al*. 2012, Yoon and Lee 2014a, Yoon and Lee 2014b, Yoon *et al*. 2015, Yoon *et al*. 2017a, Yoon *et al*. 2017b), respectively, as shown in Fig. 2(b). The meshes were assigned considering the arrangement of the ballast tanks, sufficient solution accuracy, and minimization of computational cost. For the JSM structures on the floating dock, the pontoon and column blocks are modeled by continuum mechanics based beam elements and each node block is modeled as a concentric force. Finite element models for the 8 construction steps are described in Fig. 2(c).

To express the floating condition, we employ the following principle of virtual work with hydrostatic force (Yoon *et al*. 2014),

$$\int_V \sigma_{ij}\delta e_{ij}dV + \int_V \rho_w g w \delta w dV = \int_V f_i^b \delta u_i dV + \int_S f_i^s \delta u_i dS \quad (1)$$

where V is the volume of the structure, σ_{ij} is the Cauchy stress tenser, δe_{ij} is the variation of strain tensor, ρ_w is the water density, g is the acceleration of gravity, w and δw respectively represents z-directional displacement (*i.e.,* deflection of the deck) and its variation, f_i^b and f_i^s are the body and surface force vector, δu_i is the variation of displacements, and S is the boundary surface of the structure.

Using the standard finite element procedure (Bathe 2014), the linear equation of the floating dock is obtained as

$$\mathbf{K}_{FD}\mathbf{U}_{FD} = \mathbf{F}_{FD} \quad \text{with}$$

$$\mathbf{K}_{FD} = \mathbf{K}_{deck} + \mathbf{I}_B^T\mathbf{K}_{sw}\mathbf{I}_B \quad \text{and} \quad \mathbf{F}_{FD} = \mathbf{F}_{deck} + \mathbf{I}_B^T\mathbf{F}_{sw}, \quad (2)$$

in which $\mathbf{K}_{deck}$ and $\mathbf{K}_{sw}$ respectively represent the stiffness matrix of the deck and sidewall assembled by plate and beam elements, $\mathbf{F}_{deck}$ and $\mathbf{F}_{sw}$ are the corresponding force vectors, and $\mathbf{I}_B$ is a Boolean matrix that interconnects the degrees of freedom (DOFs) between the deck plate model and the sidewall beam model. $\mathbf{K}_{deck}$ includes anisotropic material constitutive law with x- and y-directional elastic moduli of E_x and E_y. $\mathbf{F}_{deck}$ is of the self-weight of the deck (1.15 t/m^2) and weight of ballast water. $\mathbf{F}_{sw}$ is the self-weight of the sidewall (13.02 t/m).

In the present simplified finite element model, the equivalent material characteristic (*i.e*., E_x and E_y) is difficult to evaluate. To determine the appropriate material properties for the idealized model, E_x and E_y values were calibrated using the measurement results from the major strain energy mode test. A detailed description of the calibration process is given in Section 4.1.

The construction blocks of the pontoons and the columns are also modeled by beam elements to consider deflections. The linear equation of the blocks is written as

$$\mathbf{K}_{CB}\mathbf{U}_{CB} = \mathbf{F}_{CB} \quad (3)$$

where $\mathbf{K}_{CB}$, $\mathbf{U}_{CB}$, and $\mathbf{F}_{CB}$ are the stiffness matrix, displacement DOFs, and force vector, respectively, of the pontoon and column blocks assembled by beam elements. $\mathbf{F}_{CB}$ is the self-weight of the blocks as shown in Table 1. The weights of the node blocks are modeled using a concentrated load applied at the nodes (marked by blue arrows in Fig. 2). The weights of the pontoon and column blocks are modeled using distributed line loads applied at each member.

In the general finite element model, the structures are coupled through the nodal DOF-based assemblage, i.e., the finite element meshes should be regenerated according to the placement of the construction blocks. To avoid this deficiency, we employ a coupling method for not-matching nodes using localized Lagrange multipliers (Park *et al*. 2002). To connect the beam node placed at the end of the

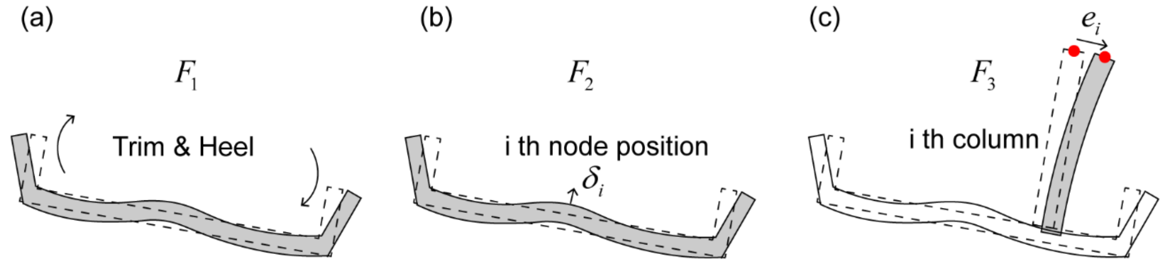

Fig. 4 Graphical illustration of the objective functions. The solid lines show a deformed configuration of the floating dock while the dotted lines represent the regressed surface of the floating dock

pontoon blocks to the corresponding plate elements of the deck, we define the interface frames as shown in Fig. 3. The respective interface frames have five nodes (four nodes corresponding to the plate nodes and one node corresponding to the beam node) of deflection displacement DOF (u_f^1, u_f^2, u_f^3, u_f^4, and u_f^5). The localized Lagrange multipliers (λ_{FD}^1, λ_{FD}^2, λ_{FD}^3, λ_{FD}^4, and λ_{CB}) represent the interaction between the interface frame and the plate and beam nodes.

The linear equations of the partitioned system are written as

$$\mathbf{K}_{FD}\mathbf{U}_{FD} = \mathbf{F}_{FD} + \mathbf{C}_{FD}\boldsymbol{\lambda}_{FD} \quad \text{and} \\ \mathbf{K}_{CB}\mathbf{U}_{CB} = \mathbf{F}_{CB} + \mathbf{C}_{CB}\boldsymbol{\lambda}_{CB} \tag{4}$$

where $\mathbf{C}_{FD}$ and $\mathbf{C}_{CB}$ are the partition-boundary extraction Boolean matrices, and $\boldsymbol{\lambda}_{FD}$ and $\boldsymbol{\lambda}_{CB}$ are the localized Lagrange multiplier vectors.

The force equilibrium for the interface frame is

$$\mathbf{L}_{FD}^T\boldsymbol{\lambda}_{FD} + \mathbf{L}_{CB}^T\lambda_{CB} = 0 \tag{5}$$

in which $\mathbf{L}_{FD}$ and $\mathbf{L}_{CB}$ are the frame-to-subdomain linking matrices.

The compatibility equation among the interface frames, corresponding plate and beam nodes are defined as

$$\mathbf{C}_{FD}\mathbf{U}_{FD} = \mathbf{L}_{FD}\mathbf{U}_f \quad \text{and} \quad \mathbf{C}_{CB}\mathbf{U}_{CB} = \mathbf{L}_{CB}\mathbf{U}_f \tag{6}$$

where $\mathbf{U}_f$ is the displacement vector for the interface frames.

Eqs. (4), (5), and (6) ultimately provide a set of coupled equations:

$$\begin{bmatrix} \mathbf{K}_{FD} & 0 & -\mathbf{C}_{FD} & 0 & 0 \\ 0 & \mathbf{K}_{CB} & 0 & -\mathbf{C}_{CB} & 0 \\ -\mathbf{C}_{FD}^T & 0 & 0 & 0 & \mathbf{L}_{FD} \\ 0 & -\mathbf{C}_{CB}^T & 0 & 0 & \mathbf{L}_{CB} \\ 0 & 0 & \mathbf{L}_{FD}^T & \mathbf{L}_{CB}^T & 0 \end{bmatrix} \begin{bmatrix} \mathbf{U}_{FD} \\ \mathbf{U}_{CB} \\ \boldsymbol{\lambda}_{FD} \\ \boldsymbol{\lambda}_{CB} \\ \mathbf{U}_f \end{bmatrix} = \begin{bmatrix} \mathbf{F}_{FD} \\ \mathbf{F}_{CB} \\ 0 \\ 0 \\ 0 \end{bmatrix} \tag{7}$$

Solving Eq. (7), we can calculate the behavior of the floating dock coupled with the construction blocks loaded at an arbitrary position on the deck of the floating dock.

3.2 Optimization method

To find the optimal ballasting plan for the given payload condition, we utilize a gradient descent algorithm (Rao 2009). The constrained optimization problem (p) can be written as

$$(p) \ \min \mathrm{F}(\vec{\mathrm{B}}) \ \ s.t. \ \ g_i(\vec{B}) \le \varepsilon_i \ \text{ for } \ i = 1,2,3 \tag{8}$$

in which $\mathrm{F}(\vec{B})$ is an objective function, $\vec{B}$ is a design variable vector, g_i are three inequality constraints, and ε_i are the allowable values for the respective constraints. To ensure hydrostatic stability and safety, the trim (g_1), heel (g_2), and draft (g_3) of the floating dock are chosen as constraints.

The design variable vector represents the amount of ballast water in each ballast tank:

$$\vec{B} = \left(B_{11}, \cdots, B_{67}\right)^T \ \text{ with } \ 0 \le B_{ij} \le B_{\max} \\ \text{for } \ j = 1, \cdots, 7 \ \text{ and } \ j = 1, \cdots, 7, \tag{9}$$

where i and j are the indexes of the ballast tanks and B_{max} is the maximum allowable amount of water.

These constraint values (i.e., g_1, g_2, and g_3) are evaluated based on the deflection ($\vec{Z}$; z-directional component of $\mathbf{U}_{FD}$ in Eq. (7)) of the floating dock as follows (Wang and Shan 2006):

$$\begin{bmatrix} 1 & g_1 & g_2 \end{bmatrix}^T = \left(\vec{X}^T\vec{X}\right)^{-1}\vec{X}^T\vec{Z} \ \text{ and} \\ g_3 = ave(\vec{\mathrm{Z}}) \ \text{ with } \ \vec{X} = \begin{pmatrix} 1 & \vec{x} & \vec{y} \end{pmatrix}, \tag{10}$$

where $\vec{x}$ and $\vec{y}$ respectively represent x and y coordinates corresponding to $\vec{Z}$. The allowable values of ε_1, ε_2 and ε_3 are assigned as 0.15 m, 0.15 m, and 0.3 m, respectively.

Three different objective functions are used to control the stability of the floating dock (F_1), the local deflections of the floating dock (F_2), and the tip tolerance of the column blocks (F_3),

$$\begin{cases} F_1(\vec{\mathrm{B}}) = \mathrm{K}_1 g_1 + K_2 g_2 + K_3 g_3, \\ F_2(\vec{B}) = \max(\vec{\delta}), \\ F_3(\vec{B}) = \sum_i^n \dfrac{e_i}{n}, \end{cases} \tag{11}$$

where K_1, K_2, and K_3 are the gain values of the trim, heel, and draft, respectively. $\vec{\delta}$ represents local deflections, n is number of columns, and e_i is the eccentricity of the column tip from the nominal position. Fig. 4 provides a graphical description of the three objective functions.

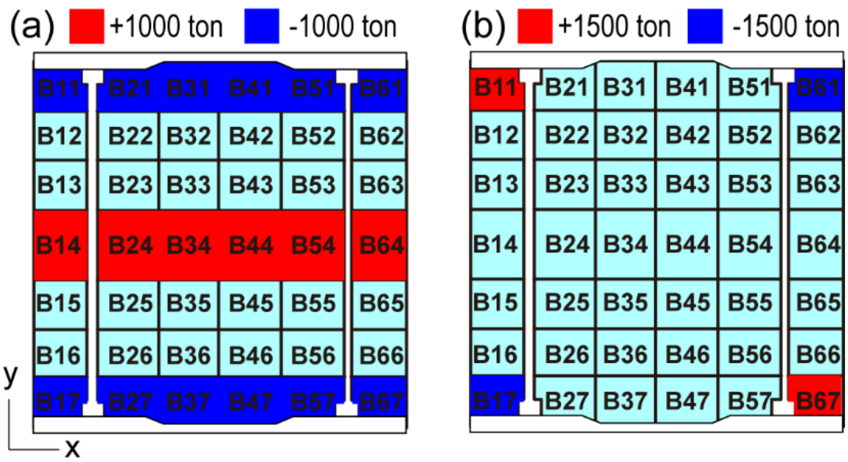

Fig. 5 Adjusted amount of the ballast water across 42 ballast tanks in the major strain energy mode test for the (a) sagging mode test and (b) twisting mode test

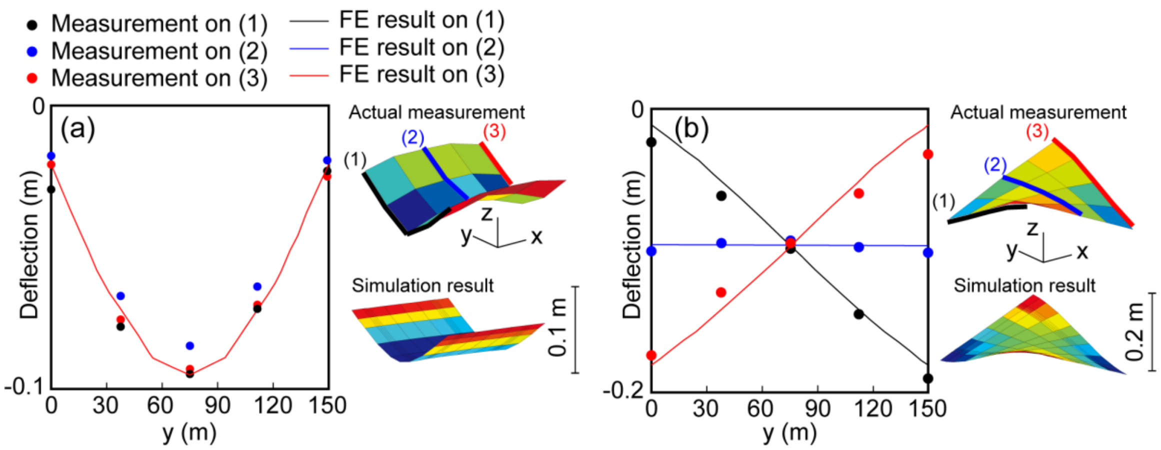

Fig. 6 Result elastic moduli calibration of E_x and E_y. Comparisons of the deflection between the actual measurement and the calibrated finite element model in the (a) sagging mode test and (b) twisting mode test

4. Calibration of the finite element model

To calibrate the behavior of the simplified finite element model to that of the actual floating dock, we performed a major strain energy mode test and updated the material properties of E_x and E_y in the model. We assessed the modal strain energy of the finite element model through eigenvalue analysis and found that the sagging and twisting modes are more dominant than the other deformation modes. Thus, we elicited two major deformation modes of sagging and twisting to the floating dock by adjusting the ballast water in the tanks as shown in Fig. 5(a) and (b). The deformation of the floating dock is measured at 25 positions (shown as red dots in Fig. 1(c)). The material properties of E_x and E_y are manually adjusted to match the behavior of the finite element model to that of the measured displacement.

Fig. 6(a) compares the deflection between the measurement and finite element model in the sagging mode test. Since the sagging mode is highly independent of y-directional bending deformation as well as to the elastic property of E_y, we determined the E_x value through manual adjustment under fixed E_y. The black, blue, and red dots in the left graph respectively represent the measured deflections on the thick black, blue, and red lines in the right configuration figure. The solid lines in the left graph indicate the deflections obtained from the finite element model. The calibrated elastic property of E_x accurately represents the sagging deformation of the finite element model compared with the actual measurement.

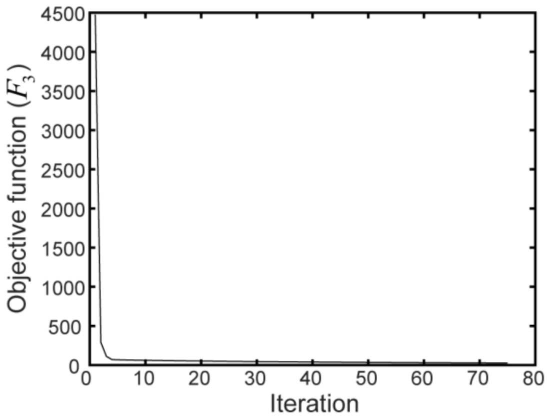

Fig. 7 Exemplar convergence of an objective function F_3 at Step 8

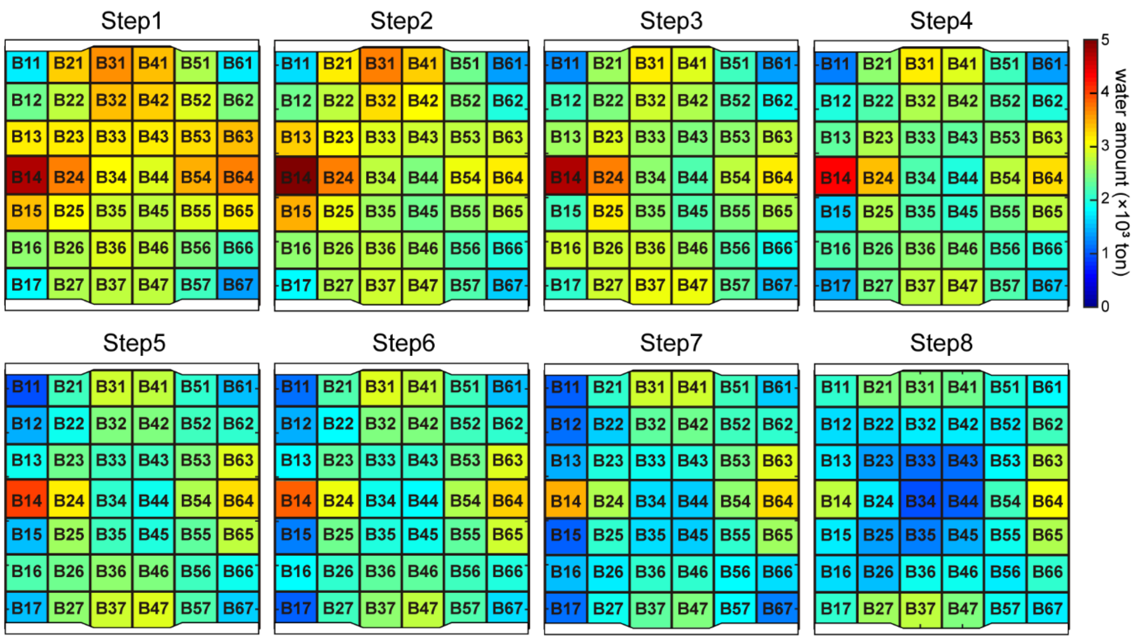

Fig. 8 Optimal distribution of ballast water for each construction step

Table 2 Additional payloads excepting the construction blocks

Erection Step	ID	Location		Weight (t)
		x (m)	y (m)	
1	KEEL BLOCKS	76.8	74.9	3175.0
	LIGHTING & PANEL BOARD	76.8	74.9	5.2
	DWT CONST.	81.8	88.5	50.0
4	CRANE FOR BENT SUPPORT	76.8	74.9	96.9
	CHERRY PICKER	76.8	74.9	66.0
5	DEBALLAST PUMP1	110.3	109.0	18.4
	DEBALLAST PUMP2	111.0	42.1	18.4
	DEBALLAST PUMP3	43.6	108.9	18.4
	DEBALLAST PUMP4	43.3	40.7	18.4
	DOCK-MASTER	76.8	74.9	160.0
	CRANE	76.8	74.9	96.9
	CHERRY PICKER	76.8	74.9	132.0
7	RGB&RGT	117.9	116.8	3940.8

Fig. 6(b) displays the deflections obtained from the actual measurement and the calibrated finite element model in the twisting mode test. In this test, we adjusted only the elastic property of E_y because the characteristic of the twisting deformation depends highly on the y-directional bending action. The dots and lines in the left graph represent the deflections obtained from the actual measurement and the calibrated finite element model, respectively, and they show good agreement.

The actual floating dock has highly complicated structural features which cannot be accounted for in the simplified finite element model. However, through the calibration procedure using experimental results, the updated finite element model was able to accurately predict the global behavior of the floating dock at a semi-real time calculation speed.

5. Optimal ballasting plan

We established ballasting plans for the eight steps of JSM construction in advance, using the developed optimization method. In addition to the construction blocks weight, various expected payloads (see Table 2) were modeled as a concentrated point load on the floating dock. The objective function of F_2 was used to calculate the ballasting plans for Steps 1–4 to secure the flatness of the workspace during construction of the pontoon and node blocks. For Steps 5–8, the objective function of F_3 was subjected to the optimization of the ballasting plans for the alignment of the column blocks. All the objective values converged under the required accuracy of 15 mm through the gradient-based algorithm. Fig. 7 shows an exemplar convergence of the objective value (F_3) during the iteration

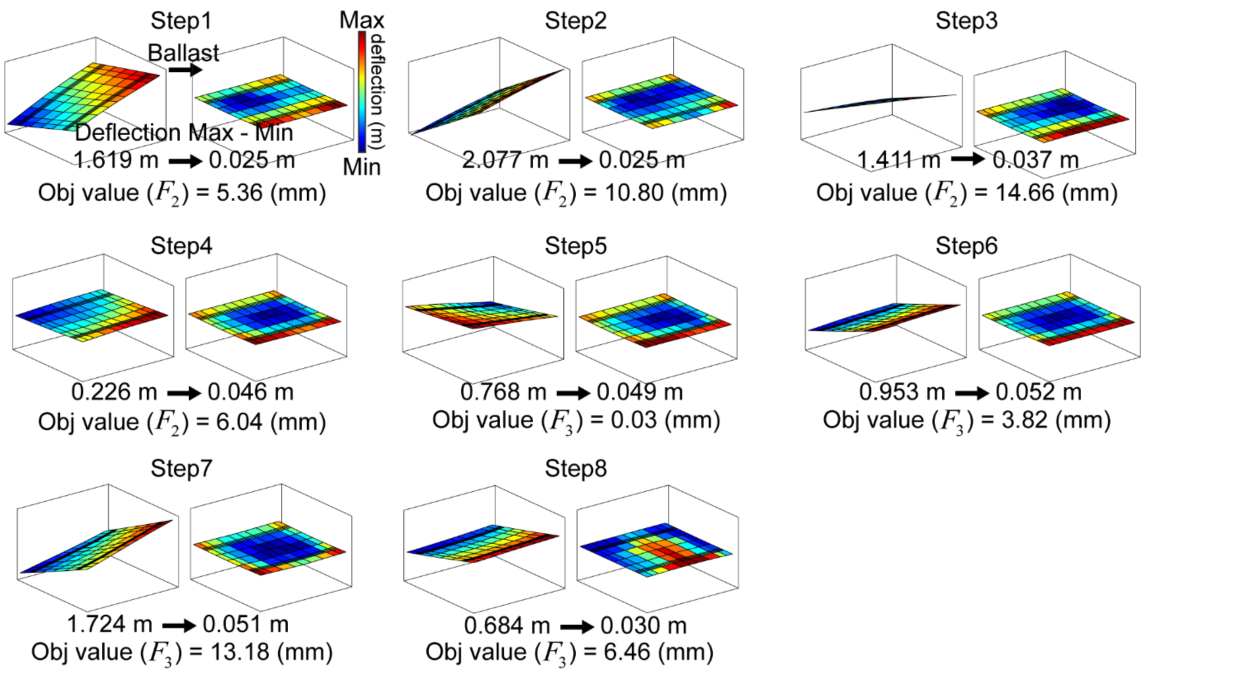

Fig. 9 Floating deck configurations obtained from the finite element model before ballasting (i.e., without water in all tanks) and after applying the optimal ballast plan in Fig. 8. The differences between the maximum and minimum deflection and objective values are also displayed for each step of construction

process to optimize the ballasting plan for Step 8 of construction.

Figure 8 displays the evaluated optimal ballasting plans for each step of construction. The required amount of water in the forty-two ballast tanks is represented by coloring within the 0 to 5,000 t range. The deformed configurations of the floating dock in each construction step are also obtained through the finite element model, as shown in Fig. 9. For each construction step, the configurations of the floating dock before ballasting (i.e., all the ballast tanks are empty) are illustrated on the left, and the deflected shapes after applying the obtained optimal ballasting plan (Fig. 8) depicted on the right side. The difference between the maximum and minimum value of deflections was also displayed before and after applying the ballasting plan. The objective values of F_2 for Step 1–4 and F_3 for Step 5–8 were successfully reduced to less than 15 mm. These results provided useful information about the overall direction for JSM construction.

6. On-site application

To manage various unpredictable situations during the actual JSM construction, the developed method was implemented as an on-site guidance system. Fig. 10 shows the graphic user interface of the developed software "Ballasting Planner" which provides the optimal distribution of ballasting water for a given payload condition as well as the floating dock deflection obtained from simulation and measurement. All the optimizations were performed using a quad-core processor (Intel(R) Core (TM) i7-7700 CPU @ 3.60 GHz, 32 GB memory, Microsoft Windows 10 64 bit). Attributed to the highly efficient

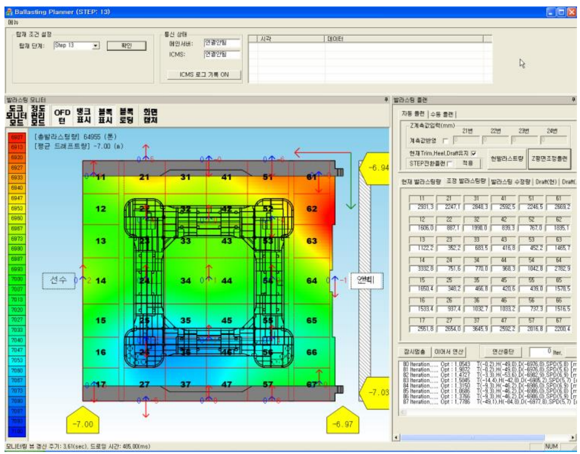
Fig. 10 GUI of the developed ballasting planner software

computational cost of the simplified finite element model used in this study, we were able to immediately calculate a new optimal ballasting plan within 5 min.

The most important feature of the on-site guidance software is its use of incremental analysis. Instead of $\mathbf{U}_{FD}$, $\mathbf{U}_{measure} + \Delta\mathbf{U}_{FD}$ are used to evaluate the objective functions, in which $\mathbf{U}_{measure}$ is obtained by interpolating the deflections measured by the 25 draft sensors and $\Delta\mathbf{U}_{FD}$ is the incremental deflection calculated using the incremental Eq. (12).

$$\mathbf{K}_{FD}\Delta\mathbf{U}_{FD} = \Delta\mathbf{F}_{FD} \tag{12}$$

Since the incremental terms $\Delta\mathbf{U}_{FD}$ and $\Delta\mathbf{F}_{FD}$ are used, we can avoid uncertainty of payloads $\mathbf{F}_{FD}$. Here, the efficacy of the developed method is demonstrated through two examples of on-site applications.

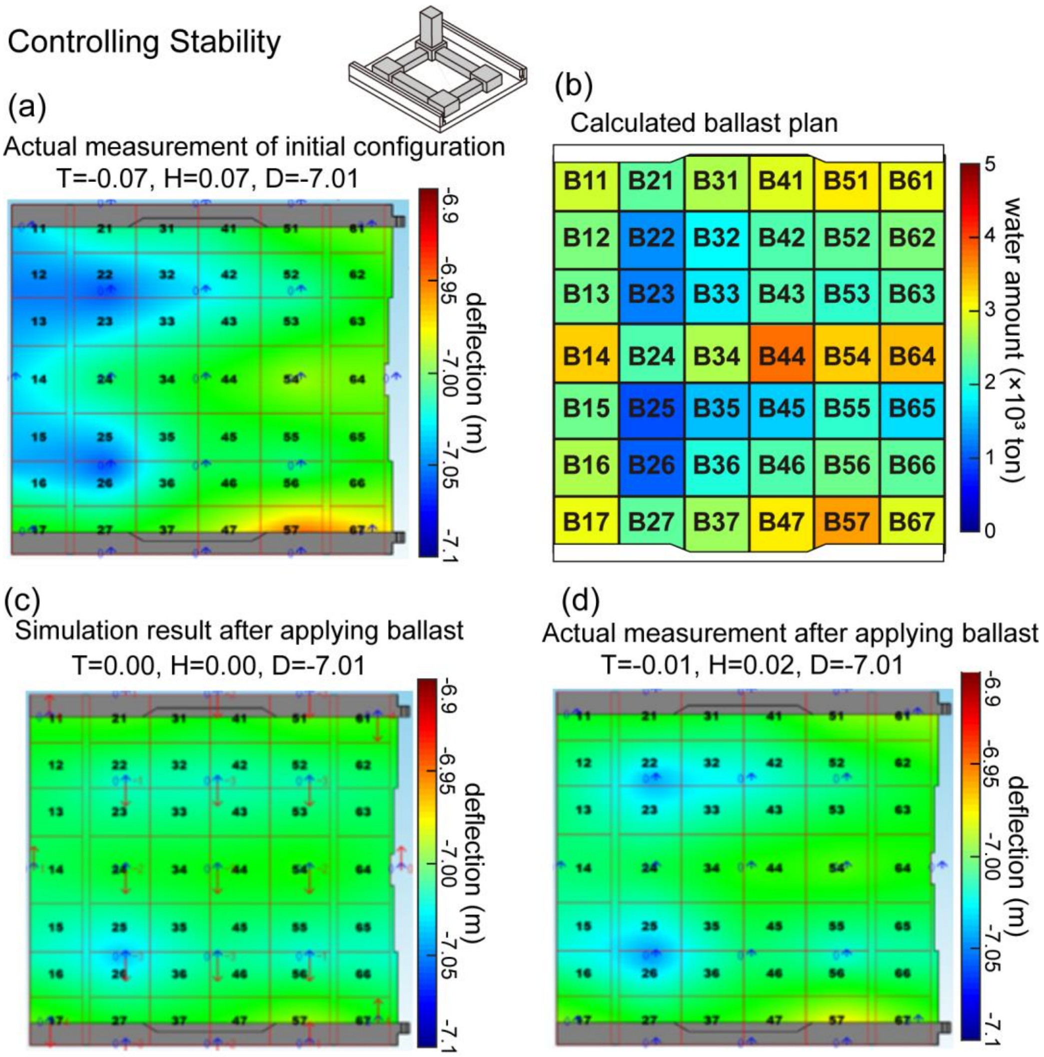

Fig. 11 Actual application result of the developed software for stability control of the floating dock (T: trim, H: heel, D: draft)

After processing Step 5, the deflection of the floating dock was measured as shown in Fig. 11(a). Considering the measured configuration, we further controlled the stability of the floating dock in terms of trim and heel by minimizing the objective function of F_1. Fig. 11(b) shows the new ballasting plan calculated from the developed on-site guidance software. Figs. 11(c) and (d) respectively, display the predicted distribution of deflection obtained from the finite element model and measured deflection after applying the new ballasting plan. The deformed configuration of the simulation result in Fig. 11(c) shows good agreement with the actual measurement in Fig. 11(d). The trim (T) and heel (H) values were successfully reduced to T=-0.01 m and H=0.02 m from T=-0.07 m and H=0.07 m in the actual measurement.

Fig. 12(a) shows the measured deflection of the floating dock after processing Step 8. The eccentricity of column tip (i.e., objective function F_3) was 0.8 m. We needed to secure more accurate erections of the column blocks, so the new ballasting plan was calculated by minimizing the objective function of F_3 based on the configurations given in Fig. 12(a). The water distribution of the new ballasting plan is displayed in Fig. 12(b). The simulation result obtained by applying the new ballasting plan is given in Fig. 12(c) and the result of the actual measurement is shown in Fig. 12(d). The objective value of F_3 was successfully reduced to 0.04 m from 0.8 m and the deformed configuration in Fig. 12(c) and (d) shows good agreement.

7. Conclusions

In this paper, a method to find the optimal ballasting plan for precise and safe operation of 2D floating docks was developed and applied to the first-ever trial of the offshore structure construction on the 2D floating dock. The flexibility of the floating dock and the construction blocks were considered using the finite element method. A gradient-based algorithm was used to search for the optimal solution for the ballasting plan. The optimal ballasting plans for the 8 construction steps of JSM (semi-submersibles and tension leg platforms, see Fig. 13) were evaluated using the developed method and were implemented as on-site guidance for managing unpredictable situations during the

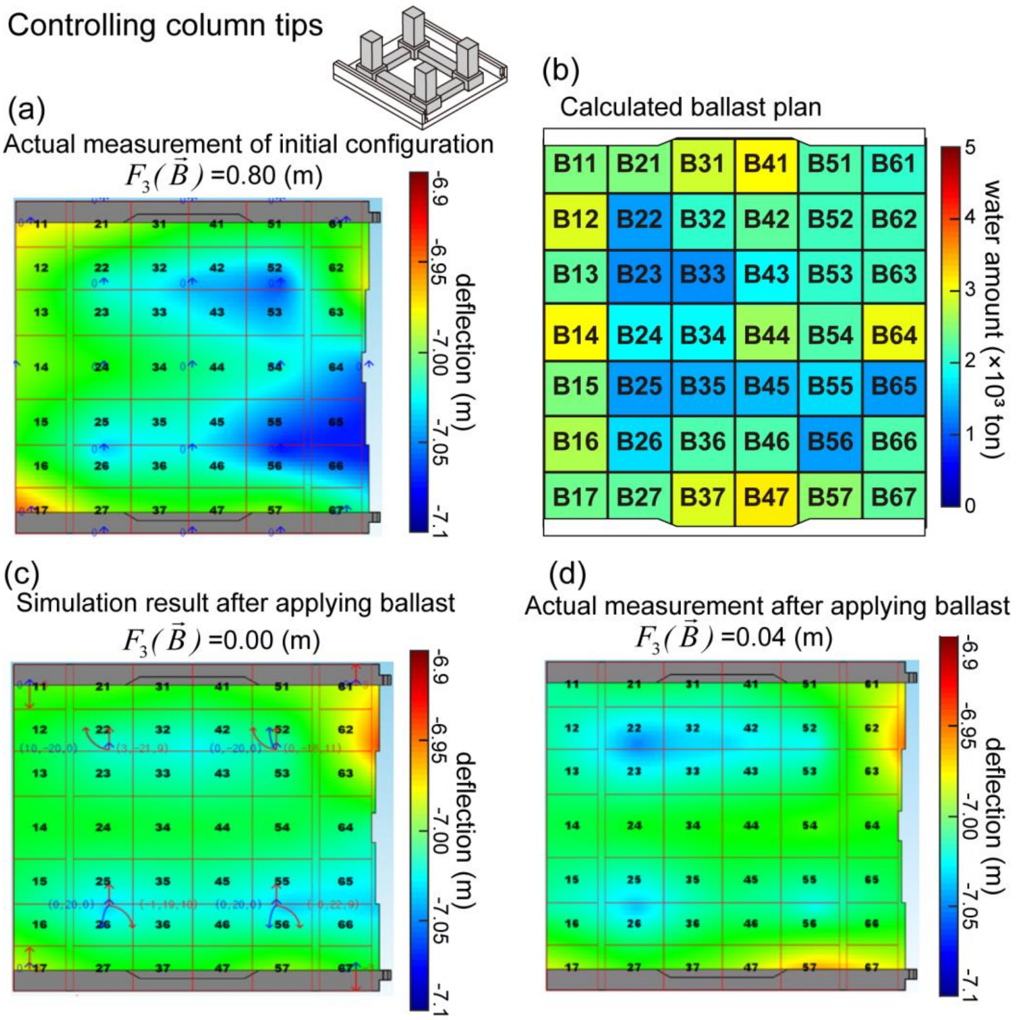

Fig. 12 Actual application result of the developed software for controlling the eccentricity of the column tip location

Fig. 13 Completed Jack and Saint Malo (JSM) in actual operation

actual JSM construction. JSM was successfully constructed on the 2D floating dock using the guidance of the developed software. The present method will be invaluable as a breakthrough technology to enable the erection of offshore structures on floating docks, which may ultimately increase productivity.

Acknowledgments

We thank Professor Phill-Seung Lee at Korea Advanced Institute of Science and Technology (KAIST) for the valuable discussion and comments. This work was performed by the Samsung Heavy Industry (SHI)–KAIST research collaboration program. This work was also supported by the “Human Resources Program in Energy Technology” of the Korea Institute of Energy Technology Evaluation and Planning (KETEP) and granted financial resources from the Ministry of Trade, Industry & Energy, Republic of Korea (No. 20184030202000). This research was a part of the project titled 'Development of rapid response technology for oil spill prevention', funded by the Ministry of Oceans and Fisheries, Korea (No.2019044019).

References

American Bureau of Shipping (2009), *Rules for Building and Classing Steel Floating Dry Docks*, American Bureau of Shipping, TX, U.S.A.

Bathe, K.J. (2014), *Finite Element Procedures*, Second Edition, Watertown, Prentice Hall, New Jersey, U.S.A.

China Classification Society (2009), *Rules for Classification of Floating Docks*, Beijing, China.

Det Norske Veritas (2012), *Rules for Classification of Floating Docks*, Høvik, Norway.

Germanischer Lloyd (1993), “Rules for Classification and Construction Floating Docks”, London, United Kingdom.

Jun, H., Yoon, K. and Lee, P.S. (2018), “The MITC3+ shell element enriched in membrane displacements by interpolation covers”, *Comput. Methods Appl. Mech. Engrg*., **337**, 458-480. https://doi.org/10.1016/j.cma.2018.04.007.

Kim, H.J., Yoon, K. and Lee, P.S. (2020), “Continuum mechanics based beam elements for linear and nonlinear analyses of multi-layered composite beams with interlayer slips”, *Compos. Struct*., **235**, 111740. https://doi.org/10.1016/j.compstruct.2019.111740.

Ko, Y., Lee, PS. and Bathe, K.J. (2016), “The MITC4+ Shell element and its performance”, *Comput. Struct*., **169**, 57-68. https://doi.org/10.1016/j.compstruc.2016.03.002.

Ko, Y., Lee, Y., Lee, P.S. and Bathe, K.J. (2017), “Performance of the MITC3+ and MITC4+ shell elements in widely-used benchmark problems”, *Comput. Struct.,* **193**, 187-206. https://doi.org/10.1016/j.compstruc.2017.08.003.

Korotaev, V.V., Pantiushin, A.V., Serikova, M.G. and Anisimov, A.G. (2016), “Deflection measuring system for floating dry docks”, *Ocean Eng*., **117**, 39-44. https://doi.org/10.1016/j.oceaneng.2016.03.012.

Kurniawan, A. and Ma, G. (2009), “Optimization of ballast plan in launch jacker load-out”, *Struct. Multidisc. Optim*., **38**, 267-288. https://doi.org/10.1007/10.1007/s00158-008-0287-7.

Lee, C. and Lee, P.S. (2019), “The strain-smoothed MITC3+ shell finite element”, *Comput. Struct.,* **223**. https://doi.org/10.1016/j.compstruc.2019.07.005.

Lee, Y.G., Lee, P.S. and Bathe, K.J. (2014), “The MITC3+ shell element and its performance”, *Comput. Struct.,* **138**, 12-23. https://doi.org/10.1016/j.compstruc.2014.02.005

Lee, Y.G., Yoon, K. and Lee, P.S. (2012), “Improving the MITC3 shell finite element by using the Hellinger-Reissner principle”, *Comput. Struct*., **110-111**, 93-106. https://doi.org/10.1016/j.compstruc.2012.07.004.

Lee, P.S. and Bathe, K.J. (2002), “On the asymptotic behavior of shell structures and the evaluation in finite element solutions”, *Comput. Struct.,* **80**, 235-255. https://doi.org/10.1016/S0045-7949(02)00009-3.

Lee, P.S. and Bathe, K.J. (2004), “Development of MITC isotropic triangular shell finite elements”, *Comput. Struct.,* **82**, 945-962. https://doi.org/10.1016/j.compstruc.2004.02.004.

Lee, P.S. and Bathe, K.J. (2005), “Insight into finite element shell discretizations by use of the ‘basic shell mathematical model’”, *Comput. Struct*., **83**, 69-90. https://doi.org/10.1016/j.compstruc.2004.07.005.

Lee, P.S. and Bathe, K.J. (2010), “The quadratic MITC plate and MITC shell elements in plate bending”, *Adv. Eng. Software*, **41**, 712-28. https://doi.org/10.1016/j.advengsoft.2009.12.011

Park, K.C., Felippa, C.A. and Rebel, G. (2002), “A simple algorithm for localized construction of non-matching structural interfaces”, *Int. J. Numer. Methods Eng.,* **53**, 2117-2142. https://doi.org/10.1002/nme.374.

Rao, S.S. (2009), *Engineering Optimization: Theory and Practice*, Fourth Ed., Wiley, New York, U.S.A. https://doi.org/10.1007/s00158-008-0287-7.

Russian Maritime Register of Shipping (2014), “Rules for Technical Supervision during Construction of Ships and Manufacture of Materials and Products for Ships”, Part V *Technical Supervision During Construction of Ship*, Russian Maritime Register of Shipping, Saint-Petersburg, Russia.

Shan, X.L., Yu, Q. and Tian, J. (2009), “Risk management of mooring operation of floating dock”, *J. Tianjin Univ*., **4**, 398-409.

Smith, D. and LeVezu, A. (2012), “Floating dock deflection management systems”, US Patent 8,155,812, April 10. https://www.google.com/patents/US8155812.

Wang, G.G. and Shan, S. (2006), “Review of metamodeling techniques in support of engineering design optimization”, *J. Mech. Des*., **129**, 370-380. https://doi.org/10.1115/1.2429697.

Yang, G., Liang, H. and Wu, C. (2013), “Deflection and inclination measuring system for floating dock based on wireless networks”, *Ocean Eng.,* **69**,1-8. https://doi.org/10.1016/j.oceaneng.2013.05.014.

Yoon, J.S., Cho, S.P., Jiwinangun, R.G. and Lee, P.S. (2014), “Hydroelastic analysis of floating plates with multiple hinge connections in regular waves”, *Mar. Struct*., **36**, 65-87. https://doi.org/10.1016/j.marstruc.2014.02.002.

Yoon, K., Lee, Y.G. and Lee, P.S. (2012), “A continuum mechanics based beam finite element with warping displacements and its modeling capabilities”, *Struct. Eng. Mech.,* **43**, 411-437. https://doi.org/10.12989/sem.2012.43.4.411.

Yoon, K. and Lee, P.S. (2014a), “Nonlinear performance of continuum mechanics based beam elements focusing on large twisting behaviors”, *Comput. Methods Appl. Mech. Engrg.,* **281**, 106-130. https://doi.org/10.1016/j.cma.2014.07.023.

Yoon, K. and Lee, P.S. (2014b), “Modeling the warping displacement fields for discontinuously varying arbitrary cross-section beams”, *Comput. Struct*., **131**, 56-69. https://doi.org/10.1016/j.compstruc.2013.10.013.

Yoon, K., Lee, P.S. and Kim, D.N. (2015), “Geometrically nonlinear finite element analysis of functionally graded 3D beams considering warping effects”, *Compos. Struct.,* **132**, 1231-1247. https://doi.org/10.1016/j.compstruct.2015.07.024.

Yoon, K., Lee, P.S. and Kim, D.N. (2017a), “An efficient warping model for elastoplastic torsional analysis of composite beams”, *Compos. Struct.,* **178**, 37-49. https://doi.org/10.1016/j.compstruct.2017.07.041.

Yoon, K., Kim, D.N. and Lee, P.S. (2017b), "Nonlinear torsional analysis of 3D composite beams using the extended St. Venant solutions", *Struct. Eng. Mech.,* **62**, 33-42. https://doi.org/10.12989/sem.2017.62.1.033.

PL